

Butane dihedral angle dynamics in water is dominated by internal friction

Jan O. Daldrop¹, Julian Kappler¹, Florian N. Brünig¹, and Roland R. Netz^{1,2}

¹Freie Universität Berlin, Department of Physics, 14195 Berlin, Germany

This manuscript was compiled on March 16, 2018

The dihedral dynamics of butane in water is known to be rather insensitive to the water viscosity, possible explanations for this involve inertial effects or Kramers' turnover, the finite memory time of friction, and the presence of so-called internal friction. In order to disentangle these factors, we introduce a method to directly extract the friction memory function from simulations in the presence of an arbitrary free-energy landscape. By analysis of the dihedral friction in butane for varying water viscosity, we demonstrate the existence of an internal friction contribution. At normal water viscosity the internal friction turns out to be eight times larger than the solvent friction and thus completely dominates the effective friction. By comparison with simulations of a constrained butane molecule that has the dihedral as the only degree of freedom, we show that internal friction comes from the six additional degrees of freedom in unconstrained butane that are orthogonal to the dihedral angle reaction coordinate. While the insensitivity of butane's dihedral dynamics to water viscosity is solely due to the presence of internal friction, inertial effects nevertheless crucially influence the resultant transition rates. In contrast, non-Markovian effects due to the finite memory time are present but do not significantly influence the dihedral barrier crossing rate of butane. These results not only settle the character of dihedral dynamics in small molecular systems such as butane, they also have important implications for the folding of polymers and proteins.

molecular friction | reaction rates | memory effects

For the understanding of conformational and biochemical reactions, a low-dimensional stochastic description in suitable reaction coordinates is a powerful approach. In particular in the context of protein folding, diffusion in a one-dimensional free-energy landscape is a prominent model to come to terms with the high-dimensional phase-space dynamics of proteins (1–3). By projection onto a one-dimensional reaction coordinate, orthogonal degrees of freedom produce effective friction and random force contributions (4, 5). These byproducts of projection cannot be neglected, since friction decisively influences reaction rates (6).

Obviously, the friction that characterizes a protein folding coordinate contains contributions from the surrounding solvent as well as from internal protein degrees of freedom (7), but it is less clear how to separately measure these two contributions (experimentally or in simulations). Typically, the prime object in protein studies concerned with friction effects is the folding time τ_{fold} . In the overdamped limit, when inertia and memory effects are neglected, τ_{fold} scales with the effective friction coefficient γ as $\tau_{\text{fold}} \sim \gamma^{-1}$ (6). By the addition of viscogenic agents the solvent viscosity η increases relative to the pure water value; assuming that solvent and internal friction are additive according to $\gamma = \gamma_{\text{sol}} + \gamma_{\text{int}}$ and furthermore that Stokes' law holds for the solvent friction contribution, $\gamma_{\text{sol}} \sim \eta$, the internal contribution γ_{int} can be obtained by linear

extrapolation of $\tau_{\text{fold}}^{-1} \sim \gamma_{\text{sol}} + \gamma_{\text{int}}$ down to vanishing solvent viscosity (7). Via this procedure, internal friction has been demonstrated for various proteins (7–16). In fact, deviations from a linear dependence $\gamma_{\text{sol}} \sim \eta$ have been experimentally observed for some proteins (9), while for other proteins no internal friction was detected at all (17). Even in simulations, where—in contrast to experiments—the water friction can be reduced and a modification of the folding free energy landscape with changing viscosity can be excluded, the extrapolation down to vanishing solvent friction is not trivial (18–22).

Furthermore, it hinges on a few critical assumptions which are not necessarily satisfied in real systems: i) It was pointed out that inertia effects lead to deviations from the simple law $\tau_{\text{fold}} \sim \gamma^{-1}$ and ultimately to Kramers turnover, which can be misinterpreted as internal friction (23–25). While one would intuitively think that the effective mass of a protein reaction coordinate is small, the balance of effective inertial and friction parameters of reaction coordinates that describe complex reactions is not really settled. ii) Friction will in general not be constant along a reaction coordinate (15, 18, 26), so the linear additivity assumption $\gamma = \gamma_{\text{sol}} + \gamma_{\text{int}}$ not necessarily holds when averaged over the reaction coordinate and needs to be checked directly. iii) Most serious are memory effects, which decisively influence barrier crossing dynamics (19, 27–29). Recently it was shown that memory effects can, depending on the value of the memory time, slow down or even accelerate barrier crossing (30), which starkly invalidates the overdamped Kramers scaling $\tau_{\text{fold}} \sim \gamma^{-1}$.

Previous theoretical approaches to internal friction are based on reaction times, they suffer from the indirect connection between transition times and friction and necessarily rely on various model assumptions (18–22) (not so different from

Significance Statement

The interpretation of rates of reactions that take place in a solvent is complicated because of the entanglement of free-energy and history-dependent friction effects. In this context, the dihedral dynamics of butane has played a paradigmatic role since it is simple yet relevant for conformational transitions in polymers and proteins. Using a novel method we directly extract the friction that governs the dihedral dynamics in butane from simulations. We show that about 89% of the total friction comes from intrinsic butane degrees of freedom that are orthogonal to the dihedral reaction coordinate and only 11% from the solvent friction. This shows that the hydrodynamic estimate of friction severely fails even in the simplest molecular reaction.

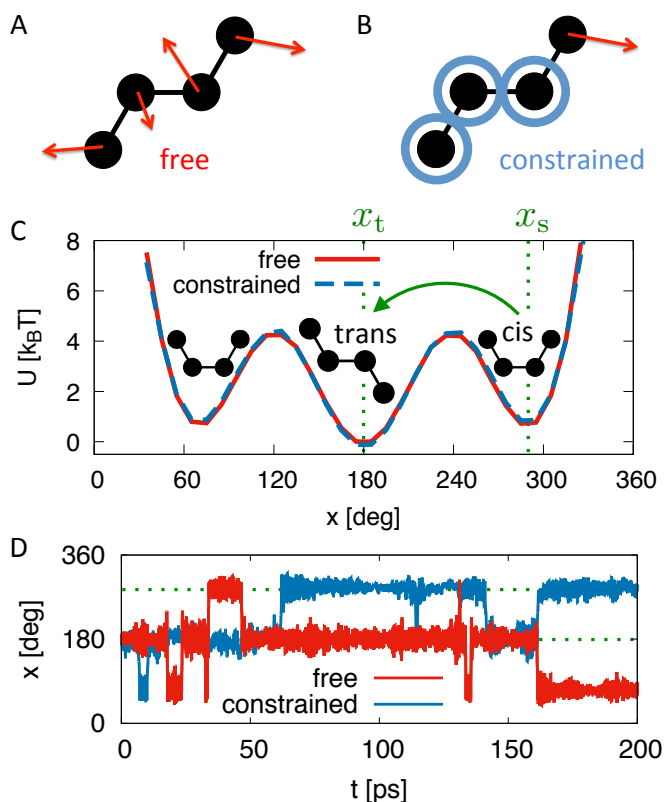
The authors declare no conflict of interest.

²To whom correspondence should be addressed. E-mail: rnetz@physik.fu-berlin.de

125 the experimental situation). Direly needed are models which
 126 allow to check for the presence of internal friction independ-
 127 ently of any theoretical assumptions that relate friction to
 128 reaction times, as well as methods to extract friction and mem-
 129 ory functions directly from simulations instead of inferring
 130 friction effects indirectly from measured reaction times.

131
 132
 133 In this paper we introduce methods to meet both chal-
 134 lenges. We consider butane, since it is the simplest molecule
 135 that shows a non-trivial conformational transition in a solvent
 136 and since it has been a testing ground for theoretical and
 137 experimental developments (31–42). Despite the fact that the
 138 solvent has a strong influence on the equilibrium properties of
 139 butane (33, 41), dihedral isomerization rates are known to be
 140 quite insensitive to the solvent viscosity (19–22, 24, 36, 43–46).
 141 The origin of the insensitivity was argued to be due to inertial
 142 and memory effects (19, 47, 48). In our work, we first simulate
 143 a single butane molecule in water and compare two scenar-
 144 ios, the free scenario, where all four carbons can freely move,
 145 subject to bond length and bond angle constraints, and the
 146 constrained scenario, where three carbons are fixed in space
 147 and only one terminal carbon can move. While the free energy
 148 landscape for the dihedral is the same in both scenarios, the
 149 transition times differ for high water viscosities (which we
 150 modify in our simulations by changing the water mass) by
 151 a factor of ten. This unequivocally demonstrates that the
 152 additional butane degrees of freedom (which are orthogonal
 153 to the dihedral angle) in the free scenario significantly change
 154 the effective friction along the reaction coordinate. Secondly,
 155 we introduce a method to extract the friction memory kernel
 156 that couples to the reaction coordinate, in our case the di-
 157 hedral angle, from simulation trajectories. A memory kernel
 158 accounts for the fact that friction on the molecular scale is
 159 not instantaneous but rather depends on the system’s history
 160 in a non-Markovian manner. Our calculated memory kernels
 161 reveal that indeed the friction substantially differs between the
 162 constrained and free butane scenarios. The friction coefficients,
 163 which follow by an integral over the memory kernels, are used
 164 to predict the transition times of the free and constrained
 165 butane scenarios in quantitative agreement with direct simu-
 166 lation results. For this we need to use reaction rate theory
 167 that accounts for inertial effects. It shows that our theoret-
 168 ical framework, which simultaneously yields reaction times
 169 as well as friction effects, is consistent. Finally, the internal
 170 friction contribution is determined by a fit of the extracted
 171 total friction versus the water viscosity: for the constrained
 172 butane the internal contribution is negligible, as expected,
 173 while for the free butane the internal contribution overwhelms
 174 the solvent contribution by a factor of eight, which explains
 175 why the butane dihedral reaction is rather insusceptible to an
 176 increase of the water viscosity.

177
 178
 179 We unambiguously show that the dihedral angle dynam-
 180 ics of a butane molecule is dominated by internal friction,
 181 which stems from the coupled dynamics of the four carbons.
 182 This demonstrates that internal friction exists already for the
 183 simplest molecular system that possesses a conformational
 184 transition, in line with previous works where dihedral angle
 185 isomerization has been argued to be a source of internal friction
 186 in protein folding (9, 20–22, 45, 46).



187
 188
 189
 190
 191
 192
 193
 194
 195
 196
 197
 198
 199
 200
 201
 202
 203
 204
 205
 206
 207
 208
 209
 210
 211
 212
 213
 214
 215
 216
 217
 218
 219
 220
 221
 222
 223
 224
 225
 226
 227
 228
 229
 230
 231
 232
 233
 234
 235
 236
 237
 238
 239
 240
 241
 242
 243
 244
 245
 246
 247
 248

Fig. 1. Schematic illustration of (A) a free butane molecule where all four carbons can move and (B) a constrained butane where three carbons are fixed in space and only one terminal carbon can move. (C) Comparison of the free energy U as a function of the dihedral angle x for the free and constrained butane solvated in SPC/E water, extracted from simulation trajectories. The starting and target angles x_s and x_t for the calculation of the *cis*-to-*trans* dihedral barrier crossing time are indicated by dotted vertical lines. (D) Typical dihedral angle simulation trajectories for free and constrained butane for elevated water viscosity $\eta = \sqrt{10}\eta_0$.

1. Results and Discussion

A. Butane dihedral barrier crossing times. In our simulations we place a single butane in a water box. We systematically vary the mass of water molecules m_w while keeping the butane mass fixed. This modifies all intrinsic water time scales and in particular also the water viscosity according to $\eta \propto \sqrt{m_w}$, but leaves all equilibrium distribution functions invariant (18). We use a united-atom force field for butane that neglects the hydrogens and approximates butane by four Lennard-Jones beads that are subject to fixed bond lengths and fixed bond angles, for water we use the SPC/E model (see Materials and Methods). We compare the free scenario, where all four butane carbons can move, with the constrained scenario, where three carbons are fixed in space and only one terminal carbon can rotate, see Fig. 1A and B for an illustration. The only degree of freedom in the constrained scenario is the dihedral angle, while in the free scenario one has six additional degrees of freedom, three translational and three orientational. The free energy profiles in the free and constrained scenarios in Fig. 1C perfectly overlap, as expected based on translational and orientational invariance of the problem.

The mean first-passage times τ_{MFP} for the *cis*-to-*trans* transition of the dihedral, as defined in Fig. 1C and extracted from the simulation trajectories as shown in Fig. 1D, are depicted as a function of the rescaled water viscosity η/η_0 in

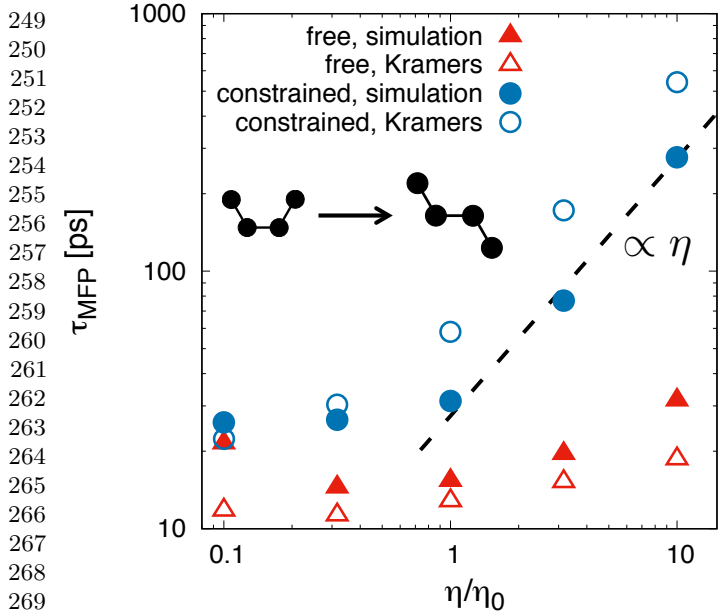


Fig. 2. Mean first passage times τ_{MFP} of the *cis*-to-*trans* transition of the butane dihedral for free (triangles) and constrained (circles) butane extracted from simulation trajectories (filled symbols) are shown as a function of the rescaled water viscosity η/η_0 , where η_0 refers to the SPC/E water viscosity. The estimates based on the Kramers formula for medium to strong friction eq. (5) are included as open symbols.

Fig. 2 for the free and constrained scenarios. Here η_0 denotes the bulk viscosity of water with the normal mass. τ_{MFP} for free butane is rather insensitive to η , in agreement with previous results (19, 36). Constrained butane behaves differently for $\eta > \eta_0$ and shows a linear increase of τ_{MFP} with η (indicated by a broken straight line), while for $\eta < \eta_0$ the results for the free and constrained scenarios are rather similar and depend only weakly on η , which will later be explained by inertial effects (i.e. Kramers turnover). The stark deviation between the free and constrained scenarios for $\eta > \eta_0$, amounting to a difference in the reaction times by a factor of ten for the highest viscosity $\eta = 10\eta_0$, is caused by the six additional degrees of freedom for free butane that are orthogonal to the dihedral angle coordinate. Since the dihedral free energy is the same for both scenarios, we conclude that the friction is different in the two scenarios and that this friction difference is caused by the additional degrees of freedom that are present in the free scenario and absent in the constrained scenario. We will later show that the difference in the total friction between the free and constrained scenarios is accompanied by an internal friction contribution for the free case.

B. Memory kernels and friction coefficients. To quantify the friction that acts on the dihedral angle, we map the dynamics of the butane dihedral angle x onto the generalized Langevin equation (GLE)

$$m\ddot{x}(t) = - \int_0^t dt' \Gamma(t') \dot{x}(t-t') - \nabla U[x(t)] + F_R(t), \quad [1]$$

where $\Gamma(t)$ denotes the memory kernel. The random force $F_R(t)$ obeys the fluctuation-dissipation theorem and satisfies $\langle F_R(t)F_R(t') \rangle = k_B T \Gamma(t-t')$. For vanishing potential, the GLE has been derived by linear projection techniques (4, 5). The mass m is an effective one and follows directly from the

simulated dihedral angle trajectory $x(t)$ via the equipartition theorem $m \langle \dot{x}^2 \rangle = k_B T$ (see Materials and Methods). The potential $U(x)$ in the GLE is in fact a free energy and follows from the simulated equilibrium probability density along the reaction coordinate, $p(x)$, as $U(x) = -k_B T \log p(x)$ and is shown in Fig. 1C. To extract $\Gamma(t)$ from simulation trajectories we extend previous methods (26, 49–51) to account for a finite potential $U(x)$. For this we multiply eq. (1) by $\dot{x}(0)$ and average to obtain

$$m \langle \dot{x}(0) \ddot{x}(t) \rangle = - \int_0^t dt' \Gamma(t') \langle \dot{x}(0) \dot{x}(t-t') \rangle - \langle \dot{x}(0) \nabla U[x(t)] \rangle, \quad [2]$$

where we used that the random force is not correlated with the initial velocity, i.e. $\langle \dot{x}(0) F_R(t) \rangle = 0$ (4). Discretizing all functions as $\Gamma_i = \Gamma(i\Delta t)$ with a timestep Δt we obtain the iteration equation

$$\Gamma_i = - \frac{1}{\omega_{i,i} \Delta t C_0^{\dot{x}\dot{x}}} \left(\sum_{j=0}^{i-1} \omega_{i,j} \Delta t \Gamma_j C_{i-j}^{\dot{x}\dot{x}} + m C_i^{\dot{x}\dot{x}} + C_i^{\dot{x}\nabla U} \right), \quad [3]$$

where we defined the correlation function $C_i^{\dot{x}\dot{x}} = \langle \dot{x}(0) \dot{x}(i\Delta t) \rangle$ (and similarly $C_i^{\dot{x}\nabla U}$ and $C_i^{\nabla U \nabla U}$) and the integration weight $\omega_{i,j} = 1 - \delta_{i,0}/2 - \delta_{i,j}/2$. The correlation function $C_i^{\dot{x}\nabla U} = \langle \dot{x}(0) \nabla U[x(i\Delta t)] \rangle$ is obtained by cubic spline interpolation of $U(x)$. In the SI we demonstrate the numerical robustness of our method. **Compared to alternative methods for the computation of memory kernels in the presence of a finite potential (26, 52), the butane molecule does not have to be constrained for our method, which excludes a possible uncontrolled systematic error caused by the confinement-dependence of molecular friction in water (53).**

The extracted memory kernels $\Gamma(t)$ for free butane in Fig. 3B are quite similar for different water viscosities, while for constrained butane the kernels in Fig. 3A differ strongly for different viscosities. In particular, for free butane the long time tail of $\Gamma(t)$, which is mostly responsible for the effective friction, is almost independent of η and oscillations appear that we associate with the presence of orthogonal degrees of freedom. In qualitative accordance with our results in Fig. 2 for the barrier crossing time, we can say that for free butane, the effective friction is less sensitive to solvent viscosity compared to constrained butane.

In Fig. 4, we show the friction coefficient γ for free and constrained butane as a function of water viscosity, which follows from an integral over the memory function according to $\gamma = \int_0^\infty dt \Gamma(t)$. For numerical integration, we fit the long time decay of $\Gamma(t)$ by an exponential function (see SI). The friction for constrained butane is linearly proportional to the solvent viscosity, as expected based on the hydrodynamic Stokes equation.

To make this more explicit, we denote the translational friction coefficient of a methyl group by $\gamma_{\text{trans}} = 6\pi\eta R_{\text{CH}_3}$. For a methyl group of radius $R_{\text{CH}_3} \approx 0.18$ nm that rotates at a fixed bond angle $\alpha = 111^\circ$ and C-C bond length $l_B = 0.15$ nm around a fixed point in space, which approximates the constrained butane case, we estimate the dihedral friction constant $\gamma = (2\pi/360)^2 (l_B \sin(\alpha))^2 \gamma_{\text{trans}} = 0.01 \cdot (\eta/\eta_0) \text{ u nm}^2/\text{deg}^2 \text{ ps}$, not so different from what we extract from the simulations in Fig. 4 for constrained butane. In contrast, the dynamics of free butane is characterized by a friction coefficient that very

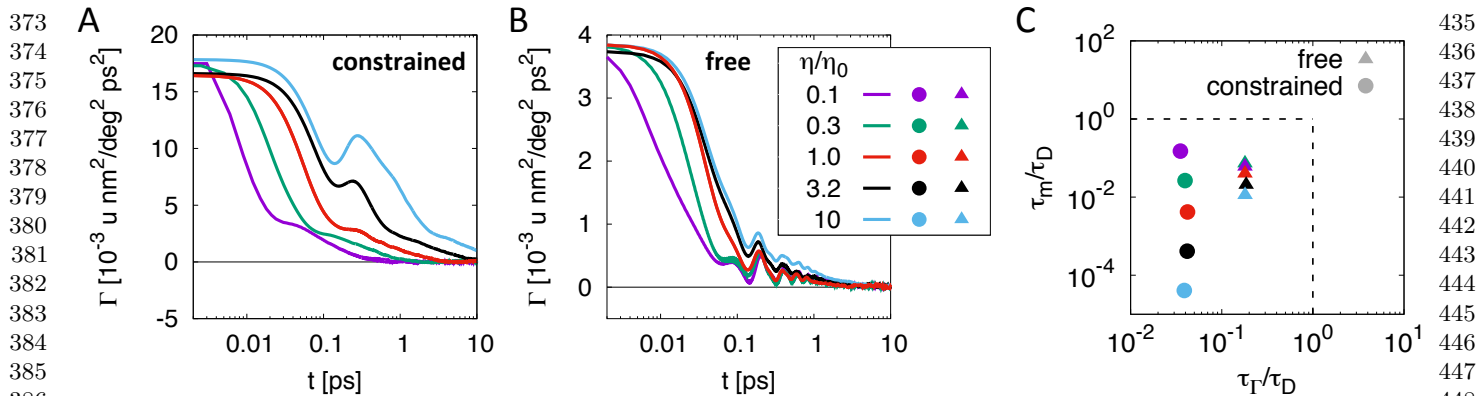


Fig. 3. Memory kernels $\Gamma(t)$ for different rescaled water viscosities η/η_0 extracted from simulation trajectories via eq. (3) for (A) constrained and (B) free butane, where η_0 denotes the SPC/E water viscosity. (C) Inertial and memory timescale ratios τ_m/τ_D and τ_Γ/τ_D calculated from the memory kernels of free and constrained butane for different viscosities, where τ_D denotes the characteristic diffusion time (same color coding as in B).

weakly depends on the water viscosity, in stark contrast to the hydrodynamic Stokes equation. Interestingly, the isomerization rate for free butane (in CCl_4) can also be estimated quite well by hydrodynamic Stokes friction, even though its viscosity dependence is not captured (36).

C. Internal versus solvent friction. We include empirical fits according to (7, 9, 12)

$$\gamma = (\eta/\eta_0) \gamma_{\text{sol},0} + \gamma_{\text{int}} \quad [4]$$

into Fig. 4 as solid lines. The fits are very good, which validates the assumption of additive solvent and internal contributions. For constrained butane we obtain $\gamma_{\text{int}} = 1.8 \cdot 10^{-4} \text{ u nm}^2/\text{deg}^2 \text{ ps}$ and $\gamma_{\text{sol},0} = 3.9 \cdot 10^{-3} \text{ u nm}^2/\text{deg}^2 \text{ ps}$, which corresponds to a ratio of $\gamma_{\text{int}}/\gamma_{\text{sol},0} = 0.05$ and shows that internal friction is negligible in this case. A small spurious internal friction contribution is in fact expected from the finite difference between the friction coefficient of immobilized and free solutes, as was recently demonstrated based on simulations of methane in water (53). In contrast, for free butane we find $\gamma_{\text{int}} = 5.2 \cdot 10^{-4} \text{ u nm}^2/\text{deg}^2 \text{ ps}$ and $\gamma_{\text{sol},0} = 6.7 \cdot 10^{-5} \text{ u nm}^2/\text{deg}^2 \text{ ps}$, and thus a ratio $\gamma_{\text{int}}/\gamma_{\text{sol},0} = 7.7$. Hence, the dynamics of free butane is dominated by internal friction effects for normal water viscosity η_0 . The substantial reduction of the solvent friction contribution $\gamma_{\text{sol},0}$ in the free case compared to the constrained case is at first sight surprising. This reduction can be rationalized by the fact that the dihedral angle for free butane is a relative coordinate that depends on the motion of all four carbons and is governed by a relative diffusion constant that results from the weighted sum of the individual carbon diffusion constants.

It remains to be checked whether the friction coefficients we extract from simulation trajectories in Fig. 4 explain the independently measured dihedral barrier crossing times in Fig. 2. This is non-trivial in the present case since, as mentioned earlier, memory and inertia effects invalidate the simple Kramers prediction $\tau_{\text{MFP}} \sim \gamma^{-1}$. To proceed, it is useful to introduce the characteristic time scales of the system. These are the inertial time $\tau_m = m/\gamma$, which measures the time at which ballistic motion crosses over to diffusive motion, the memory time $\tau_\Gamma = \gamma/\Gamma(0)$, which measures the decay time of the memory kernel, and the diffusive time $\tau_D = L^2\gamma/(k_B T)$,

which measures the free-diffusion time to advance over a characteristic angle of $L = 60^\circ$. In Fig. 3C we demonstrate that $\tau_m < \tau_D$ and $\tau_\Gamma < \tau_D$ holds for all simulation data, in which case Kramers' formula for the mean first passage time in the medium to strong friction case (6)

$$\tau_{\text{MFP}} = \frac{2\pi \omega_{\text{max}}/\omega_{\text{min}}}{[\gamma^2/4 + \omega_{\text{max}}^2]^{1/2} - \gamma/2} \exp\left(\frac{\Delta U}{k_B T}\right), \quad [5]$$

is expected to be valid. For the barrier height we extract $\Delta U = 3.7 k_B T$ from the free energy in Fig. 1C, $m\omega_{\text{max}}^2 = 6 \cdot 10^{-3} k_B T/\text{deg}^2$ and $m\omega_{\text{min}}^2 = 9 \cdot 10^{-3} k_B T/\text{deg}^2$ are the curvatures of the free energy at the maximum and minimum. The results from eq. (5) for free and constrained butane are included as open data points in Fig. 2; the comparison with the simulation data, which does not use any adjustable parameter, is quite good. This agreement is in line with previous applications of diffusion models to butane isomerization in solvent (34-37).

The simulation data in the constrained case show a shorter barrier crossing time than expected based on the Kramers formula, whereas for free butane we see the opposite. Both trends can be explained based on memory effects, since an intermediate memory time $\tau_\Gamma/\tau_D \approx 0.01 - 0.1$ significantly accelerates barrier crossing, while a longer memory time increases the barrier crossing time, as has been shown recently (30). Thus, our results for constrained butane presumably correspond to the regime where memory reduces the reaction time, while the results for free butane (which have slightly larger values of τ_Γ/τ_D , as shown in Fig. 3C) correspond to the crossover regime where the memory effect switches from acceleration to slowing down of the reaction time. The saturation of τ_{MFP} for the constrained case in the low-viscosity limit in Fig. 2 is thereby shown to be solely due to inertia effects and thus reflects Kramers turnover, this follows from the fact that the friction γ for the constrained case in Fig. 4 is roughly linear in η over the entire range of water viscosities. In contrast, the behavior of τ_{MFP} for the free case can only be explained by a combination of inertia and internal friction effects. This shows that the present simulation strategy, which compares the free and constrained scenarios and at the same time extracts memory functions, is necessary and useful.

2. Conclusions

The dihedral barrier-crossing dynamics of a constrained butane molecule, where only one carbon atom is allowed to move and thus the dihedral angle is the only degree of freedom (besides solvent degrees of freedom) is shown to be very different from the dynamics of a free butane, where a total of seven positional degrees of freedom are present. This unambiguously demonstrates that friction generated by degrees of freedom that are coupled but orthogonal to the reaction coordinate (in our case the dihedral angle) is dominant in butane. By monitoring the friction, which we directly extract from the memory kernel, as a function of the solvent viscosity, we show that orthogonal degrees of freedom significantly modify the solvent friction contribution and also produce an additional contribution which we denote, in analogy to experiments on protein folding, as internal friction, **even though this definition of internal friction is solely based on a deviation from normal Stokes-like diffusion, and therefore somewhat misleading**. The internal friction contribution in butane thus stems from the dynamic partitioning of energy over the orthogonal degrees of freedom (which in addition to the six positional also include six conjugate momentum degrees of freedom). **These six degrees of freedom correspond to three translational and three orientational degrees of freedom, which do not provide an adequate bath for the isomerization reaction in vacuum (40). Instead, collisions with the solvent molecules facilitate the energy transfer between the intramolecular modes (36).**

The weak viscosity dependence of the friction memory kernel of free butane can be understood by considering that the six orthogonal degrees of freedom together will still exchange significantly more energy with the solvent than the dihedral angle degree of freedom. Therefore, they constitute an energy bath that is rather independent of the solvent viscosity. In the SI we show that fixing one or two of the central carbon atoms of the butane molecule results into internal friction contributions of 46% and 9% at $\eta = \eta_0$ respectively. Since butane with one fixed atom has only three rotational degrees of freedom in addition to the dihedral angle, we conclude that both rotations and translations contribute to the identified internal friction mechanism.

In the GLE eq. (1), the memory kernel does not depend on the reaction coordinate x , whereas the memory kernel of frozen butane is known to have a certain conformational dependence (54), which is, however, significantly less pronounced than the differences between the kernels in Fig. 3A.

Based on our finding that already for butane, which arguably is a very simple system for which the orthogonal degrees of freedom in fact correspond to the translational and orientational degrees of freedom, internal friction dominates the dynamics, we expect that for larger and more complex molecules, which possess more orthogonal degrees of freedom, internal friction plays an even more important role for the dynamics. For macromolecular conformational transitions where the rate-limiting step involves dihedral angle isomerization (20, 24, 25, 55, 56), our findings constitute one mechanism for the emergence of internal friction effects. But other mechanisms, for example based on interactions between molecular subunits, certainly also exist.

Beyond these applications to polymers and proteins, dihedral isomerization of butane is also interesting in its own right and has been studied by two-dimensional infrared spectroscopy

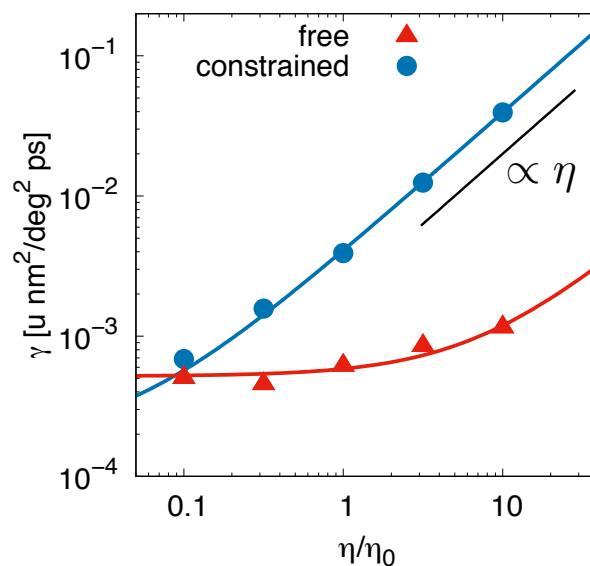


Fig. 4. Friction coefficient γ extracted from the memory kernels in Fig. 3A and B as a function of the rescaled water viscosity η/η_0 for free and constrained butane. Empirical fits according to eq. (4) (denoted by lines) yield internal-to-solvent friction ratios of $\gamma_{\text{int}}/\gamma_{\text{sol},0} = 7.7$ for free and $\gamma_{\text{int}}/\gamma_{\text{sol},0} = 0.05$ for constrained butane.

(42). The experimental dihedral isomerization time of a butane derivative solvated in CCl_4 was found to be in the 10 ps range, which agrees with predictions from classical MD simulations (36) and is similar to the simulation results we obtain here. Our analysis thus reveals that in such experiments the internal friction, which for normal water viscosity makes up about 89% of the total friction, dominates the dynamics, a fact that does not transpire from the simulations per se.

It seems difficult to derive the empirical eq. (4), according to which internal and solvent contributions, the latter being defined as the contribution that scales linearly with solvent viscosity η , are additive, from first principles. We note that the friction coefficient follows (in a non-trivial way) from the force-force autocorrelation function (53); a decomposition of the force acting on a reaction coordinate into solute and solvent contributions (which is exactly possible) would necessarily give rise to a solvent, a solute and a mixed solute-solvent contribution, and the linear additivity in eq. (4) is not obvious. The good comparison between eq. (4) and the simulation data in Fig. 4 validates the linear additivity thus only in a heuristic sense, and could break down for more complicated systems.

Materials and Methods

All simulations are carried out using the GROMACS 5.1 (57, 58) simulation package with double precision. The butane molecule is parameterized by the GROMOS (59) united atom force field, for water we use the SPC/E (60) model. All angles and bonds of water and butane are constrained to their equilibrium values using the SHAKE (61) algorithm. Real butane possesses additional degrees of freedom that we neglect in our classical simulations, namely bond angle and bond length vibrations of carbon-carbon as well as carbon-hydrogen bonds, **which have been pointed out to alter the equilibrium distribution and the dynamics of butane in liquid solvents (32)**. However, they are not expected to contribute significantly to the dynamics due to the high quantum-mechanical excitation energies for carbon-carbon bonds and due to the relatively

621 small effective mass of carbon-hydrogen bonds. We perform NVT
 622 molecular dynamics (MD) simulations and vary the water molecule
 623 mass m_w in order to change the water viscosity. For water mass
 624 larger or equal to the normal water mass, we use a time step of 2
 625 fs, for lighter water mass we lower the timestep by a factor $\eta/\eta_0 \propto$
 626 $\sqrt{m_w}$. The temperature $T = 300$ K is controlled by the velocity
 627 rescaling (62) thermostat, which is coupled only to the solvent with
 628 a time constant of $\eta/\eta_0 \cdot 1$ ps. In the SI we compare results for the
 629 memory kernels calculated from NVT and NVE simulations of a free
 630 butane molecule at a water viscosity of $\eta/\eta_0 = 0.3$ and demonstrate
 631 that the ensemble and thus the thermostat have no influence on
 632 our results. **Effective masses are extracted from the equipartition**
 633 **theorem $m\langle\dot{x}^2\rangle = k_B T$, see the SI for a short discussion. A python**
 634 **package for the memory kernel extraction is available on GitHub**
 635 **(<https://github.com/jandaldrop/memtools>).**

637 **ACKNOWLEDGMENTS.** This work was supported by the
 638 Deutsche Forschungsgemeinschaft within a grant from Sonder-
 639 forschungsbereich (SFB) 1114.

- 640 1. Bryngelson JD, Wolynes PG (1989) Intermediates and barrier crossing in a random energy
 641 model (with applications to protein folding). *J. Phys. Chem.* 93(19):6902–6915.
- 642 2. Bryngelson JD, Onuchic JN, Socci ND, Wolynes PG (1995) Funnels, pathways, and the en-
 643 ergy landscape of protein folding: A synthesis. *Proteins* 21(3):167–195.
- 644 3. Dill KA, Chan HS (1997) From Levinthal to pathways to funnels. *Nat. Struct. Biol.* 4(1):10–19.
- 645 4. Mori H (1965) Transport, Collective Motion, and Brownian Motion. *Prog. Theor. Phys.*
 646 33(3):423–455.
- 647 5. Zwanzig R (2001) *Nonequilibrium Statistical Mechanics*. (Oxford University Press).
- 648 6. Kramers HA (1940) Brownian motion in a field of force and the diffusion model of chemical
 649 reactions. *Physica* 7(4):284–304.
- 650 7. Ansari A, Jones CM, Henry ER, Hofrichter J, Eaton WA (1992) The role of solvent viscosity
 651 in the dynamics of protein conformational changes. *Science* 256(5065):1796–1798.
- 652 8. Bieri O, et al. (1999) The speed limit for protein folding measured by triplet–triplet energy
 653 transfer. *Proc. Natl. Acad. Sci. U. S. A.* 96(17):9597–9601.
- 654 9. Jas GS, Eaton WA, Hofrichter J (2001) Effect of Viscosity on the Kinetics of α -Helix and
 655 β -Hairpin Formation. *J. Phys. Chem. B* 105(1):261–272.
- 656 10. Pabit SA, Roder H, Hagen SJ (2004) Internal Friction Controls the Speed of Protein Folding
 657 from a Compact Configuration. *Biochemistry* 43(39):12532–12538.
- 658 11. Qiu L, Hagen SJ (2004) A Limiting Speed for Protein Folding at Low Solvent Viscosity. *J. Am.*
 659 *Chem. Soc.* 126(11):3398–3399.
- 660 12. Cellmer T, Henry ER, Hofrichter J, Eaton WA (2008) Measuring internal friction of an ultrafast-
 661 folding protein. *Proc. Natl. Acad. Sci. U. S. A.* 105(47):18320–18325.
- 662 13. Wensley BG, et al. (2010) Experimental evidence for a frustrated energy landscape in a three-
 663 helix-bundle protein family. *Nature* 463(7281):685–688.
- 664 14. Soranno A, et al. (2012) Quantifying internal friction in unfolded and intrinsically disordered
 665 proteins with single-molecule spectroscopy. *Proc. Natl. Acad. Sci. U. S. A.* 109(44):17800–
 666 17806.
- 667 15. Borgia A, et al. (2012) Localizing internal friction along the reaction coordinate of protein
 668 folding by combining ensemble and single-molecule fluorescence spectroscopy. *Nat Commun*
 669 3:1195.
- 670 16. Chung HS, Piana-Agostinetti S, Shaw DE, Eaton WA (2015) Structural origin of slow diffusion
 671 in protein folding. *Science* 349(6255):1504–1510.
- 672 17. Plaxco KW, Baker D (1998) Limited internal friction in the rate-limiting step of a two-state
 673 protein folding reaction. *Proc. Natl. Acad. Sci. U. S. A.* 95(23):13591–13596.
- 674 18. Schulz JCF, Schmidt L, Best RB, Dzubiella J, Netz RR (2012) Peptide Chain Dynamics in
 675 Light and Heavy Water: Zooming in on Internal Friction. *J. Am. Chem. Soc.* 134(14):6273–
 676 6279.
- 677 19. Sancho Dd, Sirur A, Best RB (2014) Molecular origins of internal friction effects on protein-
 678 folding rates. *Nat. Commun.* 5:5307.
- 679 20. Echeverria I, Makarov DE, Papoian GA (2014) Concerted Dihedral Rotations Give Rise to
 680 Internal Friction in Unfolded Proteins. *J. Am. Chem. Soc.* 136(24):8708–8713.
- 681 21. Zheng W, De Sancho D, Hoppe T, Best RB (2015) Dependence of Internal Friction on Folding
 682 Mechanism. *J. Am. Chem. Soc.* 137(9):3283–3290.
22. Zheng W, de Sancho D, Best RB (2016) Modulation of Folding Internal Friction by Local and
 Global Barrier Heights. *J. Phys. Chem. Lett.* 7(6):1028–1034.
23. Klimov DK, Thirumalai D (1997) Viscosity Dependence of the Folding Rates of Proteins. *Phys.*
Rev. Lett. 79(2):317–320.
24. Portman JJ, Takada S, Wolynes PG (2001) Microscopic theory of protein folding rates. II.
 Local reaction coordinates and chain dynamics. *J. Chem. Phys.* 114(11):5082–5096.
25. Best RB, Hummer G (2006) Diffusive Model of Protein Folding Dynamics with Kramers
 Turnover in Rate. *Phys. Rev. Lett.* 96(22):228104.
26. Straub JE, Borkovec M, Berne BJ (1987) Calculation of dynamic friction on intramolecular
 degrees of freedom. *J. Phys. Chem.* 91(19):4995–4998.
27. Grote RF, Hynes JT (1980) The stable states picture of chemical reactions. II. Rate constants
 for condensed and gas phase reaction models. *J. Chem. Phys.* 73(6):2715–2732.

28. Straub JE, Borkovec M, Berne BJ (1986) Non-Markovian activated rate processes: Compari-
 son of current theories with numerical simulation data. *J. Chem. Phys.* 84(3):1788–1794.
29. Pollak E, Grabert H, Hänggi P (1989) Theory of activated rate processes for arbitrary fre-
 quency dependent friction: Solution of the turnover problem. *J. Chem. Phys.* 91(7):4073–
 4087.
30. Kappeler J, Daldrop JO, Brüning FN, Boehle MD, Netz RR (2017) Memory-induced acceleration
 and slowdown of barrier crossing. *J. Chem. Phys.* accepted.
31. Chandler D (1978) Statistical mechanics of isomerization dynamics in liquids and the transi-
 tion state approximation. *J. Chem. Phys.* 68(6):2959–2970.
32. Chandler D, Berne BJ (1979) Comment on the role of constraints on the conformational
 structure of n-butane in liquid solvents. *J. Chem. Phys.* 71(12):5386–5387.
33. Rebertus DW, Berne BJ, Chandler D (1979) A molecular dynamics and Monte Carlo study
 of solvent effects on the conformational equilibrium of n-butane in CCl₄(a),b). *J. Chem. Phys.*
 70(7):3395–3400.
34. Montgomery JA, Chandler D, Berne BJ (1979) Trajectory analysis of a kinetic theory for iso-
 merization dynamics in condensed phases. *J. Chem. Phys.* 70(9):4056–4066.
35. Levy RM, Karplus M, Andrew McCammon J (1979) Diffusive langevin dynamics of model
 alkanes. *Chem. Phys. Lett.* 65(1):4–11.
36. Rosenberg RO, Berne BJ, Chandler D (1980) Isomerization dynamics in liquids by molecular
 dynamics. *Chem. Phys. Lett.* 75(1):162–168.
37. Knauss DC, Evans GT (1980) Liquid state torsional dynamics of butane: The Kramers rate
 and the torsion angle correlation times. *J. Chem. Phys.* 73(7):3423–3429.
38. Evans GT (1980) Momentum space diffusion equations for chain molecules. *J. Chem. Phys.*
 72(7):3849–3858.
39. Pratt LR, Rosenberg RO, Berne BJ, Chandler D (1980) Comment on the structure of a simple
 liquid solvent near a n-butane solute molecule. *J. Chem. Phys.* 73(2):1002–1003.
40. Berne BJ, De Leon N, Rosenberg RO (1982) Isomerization dynamics and the transition to
 chaos. *J. Phys. Chem.* 86(12):2166–2177.
41. Rosenberg RO, Mikkilineni R, Berne BJ (1982) Hydrophobic effect on chain folding. The trans
 to gauche isomerization of n-butane in water. *J. Am. Chem. Soc.* 104(26):7647–7649.
42. Zheng J, Kwak K, Xie J, Fayer MD (2006) Ultrafast Carbon-Carbon Single-Bond Rotational
 Isomerization in Room-Temperature Solution. *Science* 313(5795):1951–1955.
43. Kuhn W, Kuhn H (1946) Modellmässige Deutung der inneren Viskosität (der Formzähigkeit-
 skonstante) von Fadenmolekeln I. *Helv. Chim. Acta* 29(3):609–626.
44. Khatri BS, McLeish TCB (2007) Rouse Model with Internal Friction: A Coarse Grained Frame-
 work for Single Biopolymer Dynamics. *Macromolecules* 40(18):6770–6777.
45. Soranno A, et al. (2017) Integrated view of internal friction in unfolded proteins from single-
 molecule FRET, contact quenching, theory, and simulations. *Proc. Natl. Acad. Sci. U. S. A.*
 114(10):E1833–E1839.
46. Avdoshenko SM, Das A, Satija R, Papoian GA, Makarov DE (2017) Theoretical and com-
 putational validation of the Kuhn barrier friction mechanism in unfolded proteins. *Sci. Rep.*
 7.
47. Pastor RW, Karplus M (1989) Inertial effects in butane stochastic dynamics. *J. Chem. Phys.*
 91(1):211–218.
48. Zuckerman DM, Woolf TB (2002) Transition events in butane simulations: Similarities across
 models. *J. Chem. Phys.* 116(6):2586–2591.
49. Berne BJ, Harp GD (1970) On the Calculation of Time Correlation Functions in *Advances in*
Chemical Physics, eds. Prigogine I, Rice SA. (John Wiley & Sons, Inc.), pp. 63–227.
50. Lange OF, Grubmüller H (2006) Collective Langevin dynamics of conformational motions in
 proteins. *J. Chem. Phys.* 124(21):214903.
51. Shin HK, Kim C, Talkner P, Lee EK (2010) Brownian motion from molecular dynamics. *Chem.*
Phys. 375(2–3):316–326.
52. Berne BJ, Tuckerman ME, Straub JE, Bug ALR (1990) Dynamic friction on rigid and flexible
 bonds. *J. Chem. Phys.* 93(7):5084–5095.
53. Daldrop JO, Kowalik BG, Netz RR (2017) External Potential Modifies Friction of Molecular
 Solutes in Water. *Phys. Rev. X* 7(4):041065.
54. Wan SZ, Xu YW, Wang CX, Shi YY (1995) Analysis of friction kernels for n-butane isomeriza-
 tion in water by the generalized Langevin equation. *J. Chem. Phys.* 102(12):4976–4980.
55. Kuhn W, Kuhn H (1945) Bedeutung beschränkt freier Drehbarkeit für die Viskosität und Strö-
 mungsdoppelbrechung von Fadenmoleküllösungen I. *Helv. Chim. Acta* 28(1):1533–1579.
56. Guo Z, Thirumalai D (1995) Kinetics of protein folding: Nucleation mechanism, time scales,
 and pathways. *Biopolymers* 36(1):83–102.
57. Hess B, Kutzner C, van der Spoel D, Lindahl E (2008) GROMACS 4: Algorithms for Highly
 Efficient, Load-Balanced, and Scalable Molecular Simulation. *J. Chem. Theory Comput.*
 4(3):435–447.
58. Abraham MJ, et al. (2015) GROMACS: High performance molecular simulations through
 multi-level parallelism from laptops to supercomputers. *SoftwareX* 1–2:19–25.
59. Oostenbrink C, Villa A, Mark AE, Van Gunsteren WF (2004) A biomolecular force field based
 on the free enthalpy of hydration and solvation: The GROMOS force-field parameter sets
 53a5 and 53a6. *J. Comput. Chem.* 25(13):1656–1676.
60. Berendsen HJC, Grigera JR, Straatsma TP (1987) The missing term in effective pair poten-
 tials. *J. Phys. Chem.* 91(24):6269–6271.
61. Ryckaert JP, Cicotti G, Berendsen HJC (1977) Numerical integration of the cartesian equa-
 tions of motion of a system with constraints: molecular dynamics of n-alkanes. *J. Comput.*
Phys. 23(3):327–341.
62. Bussi G, Donadio D, Parrinello M (2007) Canonical sampling through velocity rescaling. *J.*
Chem. Phys. 126(1):014101.
63. (2018) memtools (<https://github.com/jandaldrop/memtools>). DOI: XXXXXXXX.